Supporting Information

A new class of molecular electrocatalysts for hydrogen evolution: catalytic activity of $M_3N@C_{2n}$ (2n=68, 78, 80) fullerenes

Alain R. Puente Santiago,[a*] Mohamed Fathi Sanad,[a,b] Antonio Moreno-Vicente,[c] Md Ariful Ahsan,[a] Maira R. Cerón,[d] Yang-Rong Yao,[a] Sreeprasad T. Sreenivasan, [a] Antonio Rodriguez-Fortea,[c] Josep M. Poblet,[c*] Luis Echegoyen[a*]

[a]Department of Chemistry, University of Texas at El Paso, 500 W. University Avenue, El Paso, Texas 79968, USA.

[b] Department of Environmental Sciences and Engineering, University of Texas at El Paso, 500 W. University Avenue, El Paso, Texas 79968, USA.

[c]Departmento de Química Física i Inorgànica, Universitat Rovira i Virgili, Marcel·lí Domingo 1, 43007, Tarragona, Spain.

[d] Lawrence Livermore National Laboratory 7000 East Ave, Livermore, CA 94550, USA.

Synthesis of the EMFs

Isomerically pure samples of $Sc_3N@C_{2n}$ (2n=68, 78 and 80) were obtained using a combination of a non-chromatographic redox-based method and HPLC developed in our laboratories.[1,2] The other endohedral compound samples ($M_3N@C_{80}$, M=Y, Lu, and Gd) were purchased from Luna Nanoworks and used directly as received after checking their purity by MALDI MS and HPLC. The structural characterization of these compounds has been also published elsewhere.[3-5]

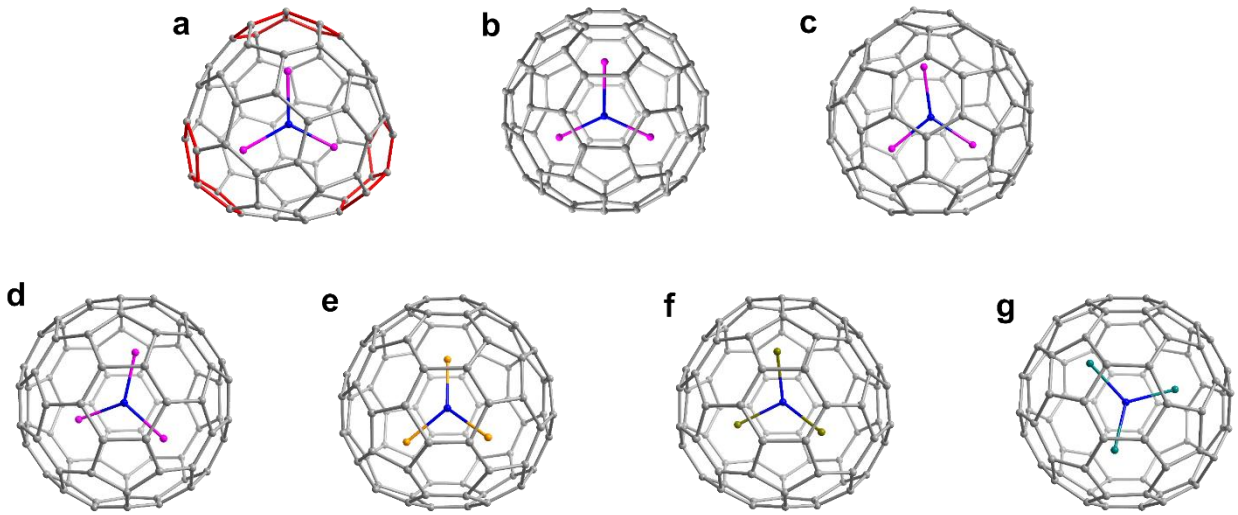

Figure S1. A ball-and-stick representation of **a)** $Sc_3N@D_3(6140)$-C_{68}, **b)** $Sc_3N@D_{3h}(5)$-C_{78}, **c)** $Sc_3N@D_{5h}(6)$-C_{80}, **d)** $Sc_3N@I_h(7)$-C_{80}, **e)** $Y_3N@I_h(7)$-C_{80}, **f)** $Gd_3N@I_h(7)$-C_{80}, and **g)** $Lu_3N@I_h(7)$-C_{80} endohedral fullerenes.

Electrochemical characterization of the EMFs

Electrochemical measurements were performed in a three-electrode system at an electrochemical workstation (CHI 660D). 5 μL of each EMF toluene solution (containing 0.05 mg/mL of catalyst) was deposited onto a 3 mm diameter glassy carbon electrode to reach a loading of approximately 3.57 $\mu g \cdot cm^{-2}$. LSVs with scan rate of 2 $mV \cdot s^{-1}$ were performed in 0.5 M H_2SO_4 (purged with pure Ar) using Ag/AgCl (in 3 M KCl solution) electrode as the reference electrode, a graphite rod as the counter electrode and the glassy carbon electrode as the working electrode. All the LSV measurements were repeated at least 3 times to assure reproducibility. All the potentials were calibrated to a reversible hydrogen electrode (RHE).

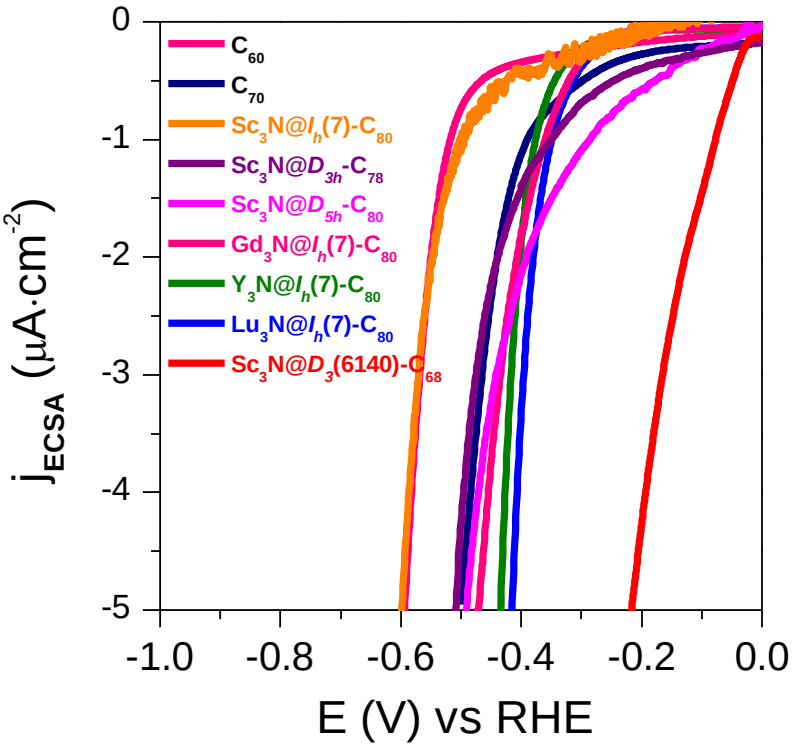

Figure S2. ECSA-normalized LSVs of the EMF catalysts.

Double layer capacitance measurements

The electrochemical double-layer capacitances of the EMFs were carried out from 0 to 0.20 V (vs RHE) in a Ar-saturated 0.5 M H_2SO_4 solution at different scan rates (20, 40, 100, 150 and 200 mV/s). The difference between the anodic and cathodic current (at 0.12 V vs RHE) were plotted against the scan rate to obtain a linear relationship and the slopes correspond to the specific capacitances of the molecular electrocatalysts.[6]

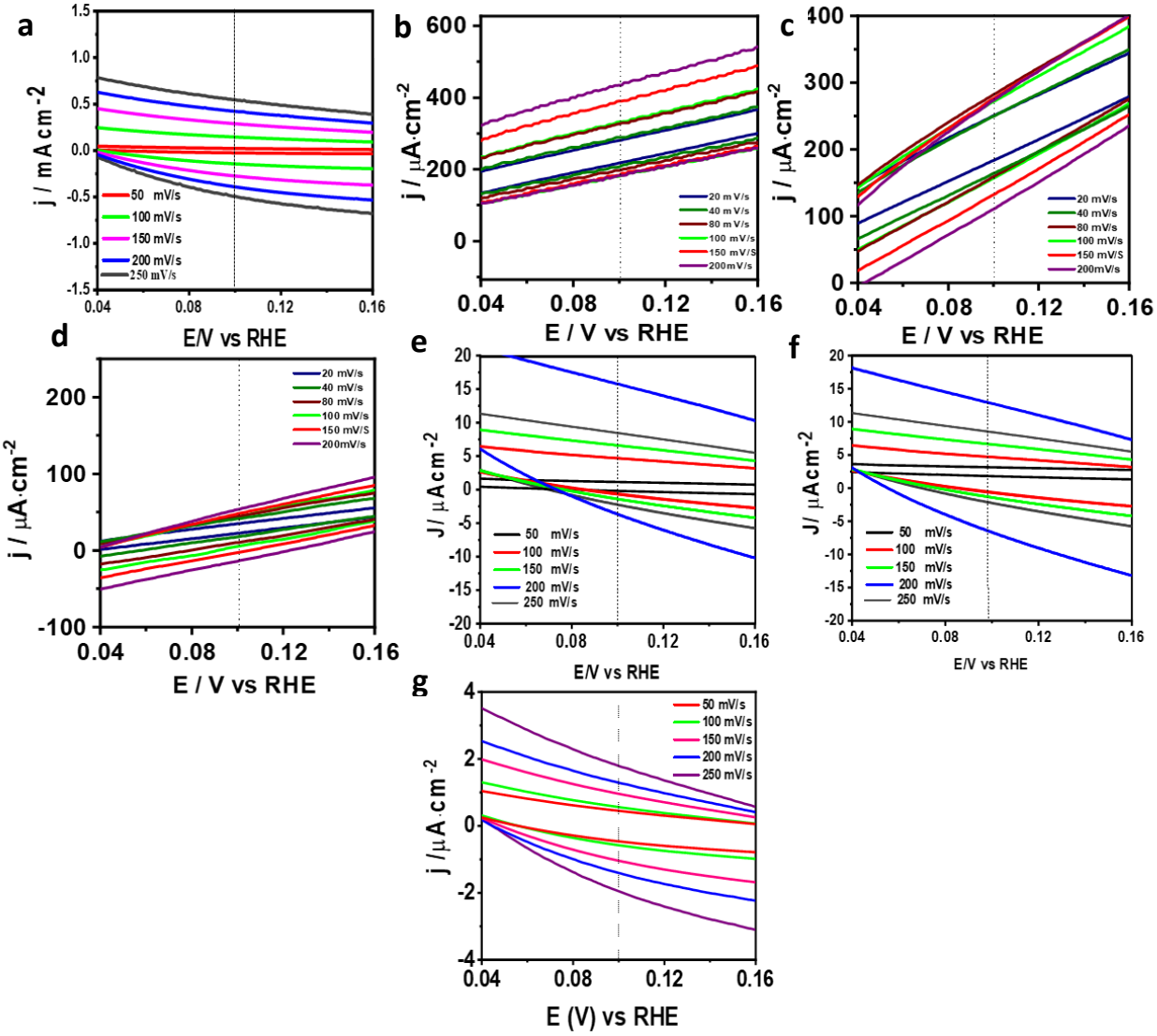

Figure S3. Double layer capacitance measurements for **a)** $Sc_3N@D_3(6140)$-C_{68}, **b)** $Lu_3N@I_h(7)$-C_{80}, **c)** $Y_3N@I_h(7)$-C_{80}, **d)** $Sc_3N@D_{5h}(6)$-C_{80}, **e)** $Gd_3N@I_h(7)$-C_{80} , **f)** $Sc_3N@D_{3h}(5)$-C_{78} and **g)** $Sc_3N@I_h(7)$-C_{80}.

Turnover frequency number (TOF) estimation for the $Sc_3N@D_3(6140)$-C_{68} catalysts

The TOF value of $Sc_3N@D_3(6140)$-C_{68} was estimated using the following equation at -0.40 V vs RHE:

$$TOF = \frac{|j|A}{mFN}$$

where N is the quantity of active sites, j is the current density at a fixed potential, A is the geometrical surface area of the electrode (0.0707 cm^2) and F is the Faradic constant (96485 C/mol). A factor of 1/m is presented, considering that m electrons are consumed to form one H_2.

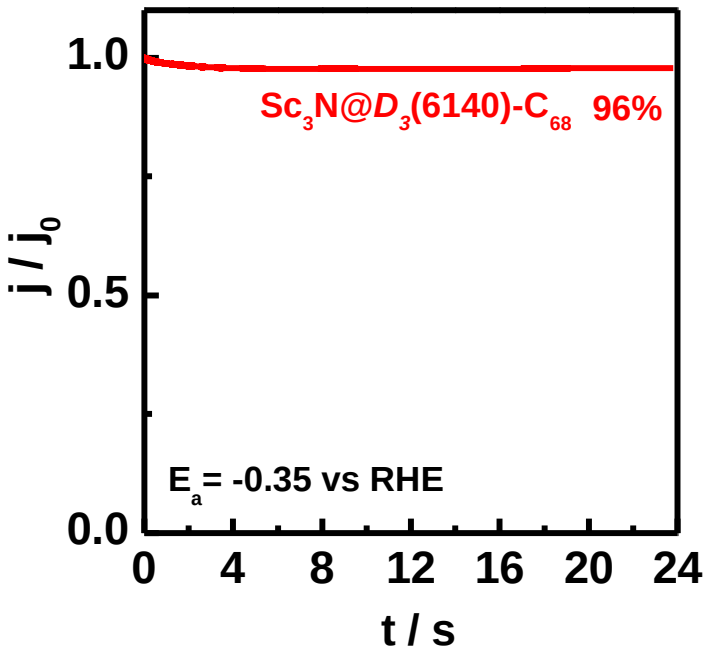

Figure S4. I-t curves for $Sc_3N@D_3(6140)$-C_{68} at -0.35 V vs RHE after 24h.

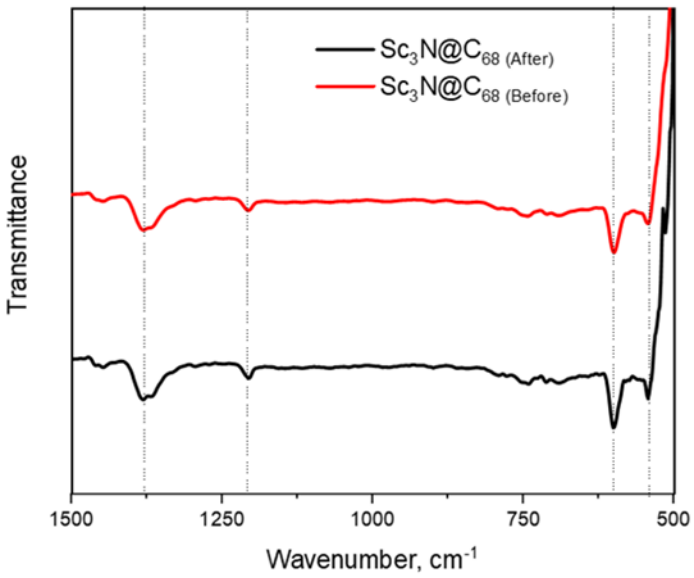

Figure S5. Typical IR spectra for the $Sc_3N@D_3(6140)$-C_{68} catalyst before and after the chronoamperometric study represented in **Figure S4**.

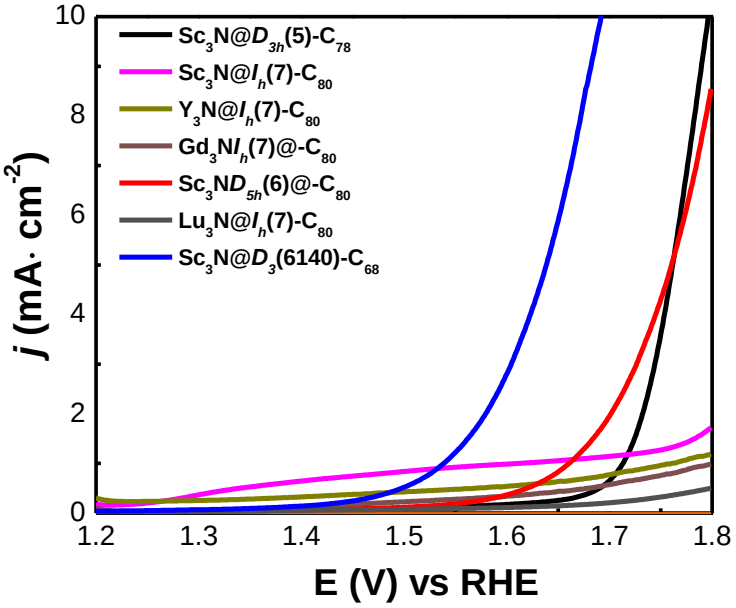

Figure S6. OER polarization curves for the EMF catalysts.

Overall water splitting device application.

The overall water splitting experiments were conducted following a previously published method.[7]

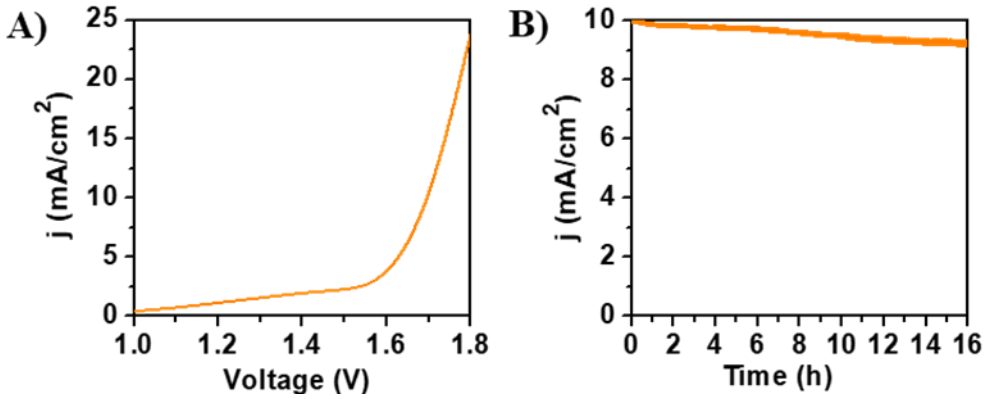

Figure S7. a) LSV curve of the overall water-splitting system using $Sc_3N@D_3(6140)$-C_{68} as both anode and cathode in a 1 M KOH electrolyte solution and b) Chronoamperometric test of the $Sc_3N@D_3(6140)$-C_{68} electrocatalyst for water electrolysis process at 1.69 V for 16 h.

Band gap calculations and M-S study

A semiconductor nanomaterial bandgap can either be direct, indirect, direct forbidden, or indirect forbidden allowed transition depending on the material type. The universal UV–vis technique for optical bandgap measurement allows for estimation in both direct and indirect energy gap materials. The optical absorption of semiconductor nanomaterials is derived from models in which the electrons receive a quantum mechanics approach, and classical EM waves describe the photons. The optical absorption coefficientα, at the photon energy E of an electron excited from the valence (V_B) to the conduction (C_B) band, is given by the transition rate;

$$W_{CB-VB} = \frac{2\pi}{h}(M)^2 g(E)$$

where M and $g_{(E)}$ stand for the (coupling) transition matrix element and the (joint electron-hole) density of states.

To determine the flat-band potentials of the samples relative to Ag/AgCl reference electrode, the Mott-Schottky equation (depending on the free charge carrier density) was obtained from the Poisson's equation for Schottky barriers at semiconductor/electrolyte heterojunctions with the assumptions of ideal blocking features of the border, absence of surface states, dominant space charge layer capacitance rather than Helmholtz layer capacitance, excellent planar interface, zero

resistance of the electrocatalysts and electrolyte. The ideal Mott-Schottky equation obtained by applying Boltzmann statistics is expressed as:

$$\frac{1}{C^2} = \frac{2}{e\varepsilon_0 \varepsilon N_d A^2}\left(V - V_{FB} - \frac{k_B T}{e}\right)$$

Where C is the charge layer capacitance, ε_0 is the vacuum permittivity, ε_r is the static dielectric constant. N_d is the charge density in the space charge region, A is the exposed area of the sample to the electrolyte, V is the applied potential concerning the reference electrode, V_{fb} is the flat band potential, kB is the Boltzmann constant, T is the absolute room temperature, and e is the elementary charge of an electron.

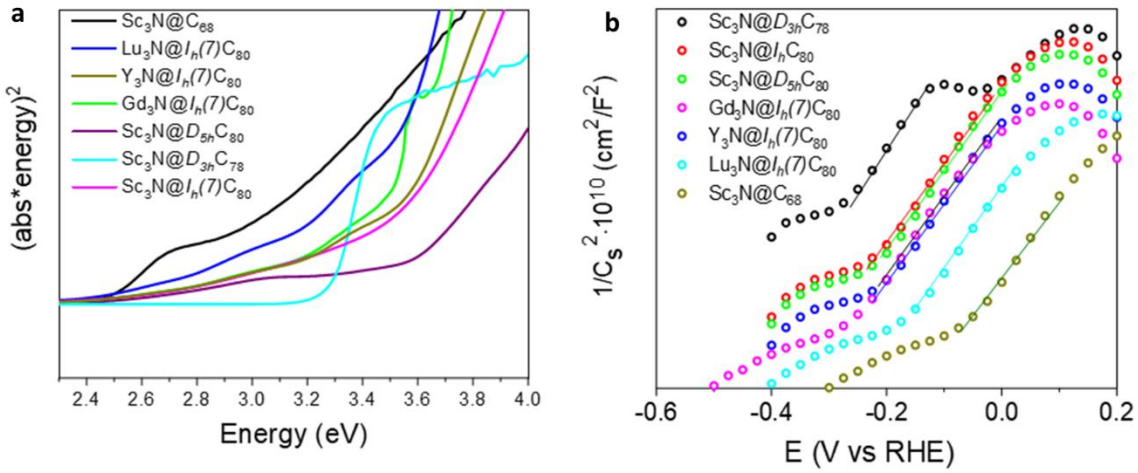

Figure S8. a) Tauc's plots of the endohedral fullerenes compounds and **b)** Mott-Schottky (M-S) plots of the seven EMFs nanocatalysts in 0.5 M H_2SO_4.

Computational details

All electronic structure calculations were performed using density functional theory (DFT) method with a generalized gradient approximation (GGA) and Perdew-Burke-Ernzerhof (PBE) exchange-correlation functional as implemented in Amsterdam density functional code (ADF2017).[8] Triple-ζ polarization (TZP) basis sets were used to describe the electrons. Frozen cores consisting of (i) the 1s shell for C and N; (ii) the 1s to 2p shells for Sc were used. Relativistic corrections were included by means of the ZORA formalism. In addition, the Grimme Dispersion D3 method was considered.[9]

Cationic fullerenes were stabilized using water as solvent by conductor-like screening model (COSMO).[10, 11] This relatively crude approach allows to place the frontier molecular orbitals at the right energy level for anionic and cationic species, which

are too high or too deep, respectively, in the gas phase.[12] Thus, the redox properties of endohedral fullerenes or polyoxoanions can be well reproduced, and even complex processes such as heterogenized polyoxometalate catalysts for water oxidation can be modeled.[13]

The protonation energies for C_{60} and clusterfullerenes were estimated from the calculations of the species in water using the COSMO approach. $\Delta E(H2)$ and $\Delta G(H2)$ were also computed in aqueous solution. However, ΔGH^* values were determined in the gas phase to be comparable to previous results. No significant differences were observed between the values in solution and in the gas phase when only neutral species are involved, as for $\Delta G(H2)$ and ΔG_{H^*}.

HER mechanism for fullerenes and endofullerenes

Scheme S1 compiles a plausible electron reduction and protonation mechanism of two IPR (C_{60} and $Sc_3N@C_{80}$) and one non-IPR fullerene, compatible with the computational energies obtained and the observed experimental results. C_{60} has a very low tendency to adsorb a proton, thus initially it is necessary to apply a potential to promote the adsorption of a H^+. In fullerenes containing metals in their interior, the situation is completely different thanks to guest-to-host electron transfer. In scandium nitride clusterfullerenes, there is a 6e transfer from the internal guest to the carbon surface, which favors the attachment of protons. We have estimated that $Sc_3N@C_{68}$ can be easily protonated twice, when it comes into contact with an acid solution, forming cationic species $Sc_3N@C_{68}H_2^{2+}$. The protonation energies (ΔE_{H+}) were computed to be -0.76 and -0.66 eV for the first and second proton, respectively. Then, $Sc_3N@C_{68}H_2^{2+}$ can be reduced at very low potential giving species $Sc_3N@C_{68}H_2$. From this species, the release of H_2 is an exergonic process with a $\Delta G(H_2)$ = -0.20 eV (Table S3). Given the protonation energies of $Sc_3N@C_{68}H_2$ and its deep LUMO, it is expected that the clusterfullerene can be easily reduced and protonated several times. The second one-electron reduction step likely determines the observed onset potentials for all the process.

For $Sc_3N@C_{80}$, the activation process of the catalyst is slightly different. Hence, while the monoprotonation is estimated to be quite favorable (ΔE_{H+}=-0.53 eV), the adsorption of a second proton on its surface is much less feasible, ΔE_{H+}=-0.09 eV (Table 1). Given that the $Sc_3N@C_{80}H^+$ fullerene can be reduced at lower potential than the bare C_{60}, we assume that the $Sc_3N@C_{80}H^+$ -> $Sc_3N@C_{80}H$ step determines the onset potential for this electrocatalyst. The relative reduction potentials computed for $Sc_3N@C_{68}$ (0.0 V) $Sc_3N@C_{80}$ (-0.42 V) and C_{60} (-0.58 V) agree with experimental trends for the three electrocatalysts. It is worth noting that our reduction potentials are somewhat more positive than the experimental values, probably because the

environment of the fullerene in the catalyst is different from that of a fullerene in a solution. Additional computational studies are underway on these and other endofullerenes to gain a deeper understanding of the full HER mechanism.

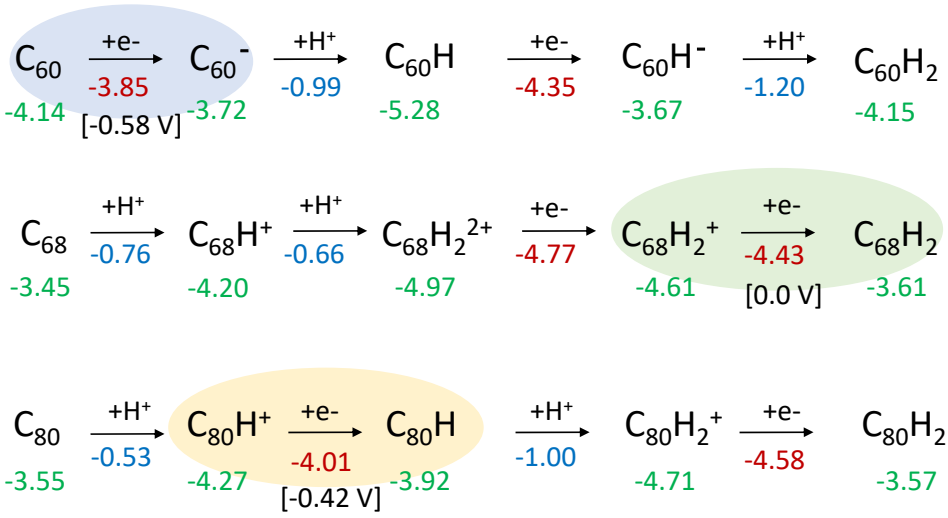

Scheme S1. Postulated HER mechanism for the initial steps for C_{60}, $Sc_3N@C_{68}$ and $Sc_3N@C_{80}$ endofullerenes. The steps that are supposed to determine the overpotential are highlighted. Reduction and protonation energies are given in eV, whereas the overpotentials relative to $Sc_3N@C_{68}$ are in V. The pronation and one-electron reduction energies of the fullerenes are in blue and red, respectively. The energy of the LUMO for all species are in green. All values were computed assuming the species in water solution

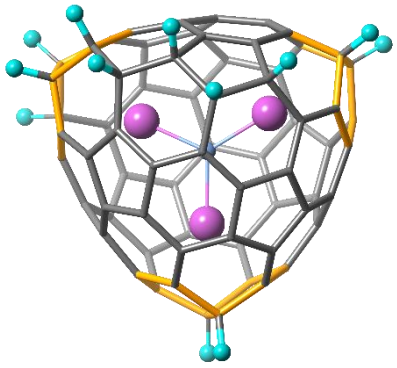

Figure S9. 3D representation for $Sc_3N@_{68}H_{12}$ computed in gas phase. This structure was used to determine chemisorption free energy ΔG_{H^*} as $\Delta G_{H^*} = (1/m)\, E(M@C_{2n}H_m) - E(M@C_{2n}) - m/2\, E(H_2) + 0.24$.

Table S1. Comparison of the onset potential of $Sc_3N@D_3(6140)$-C_{68} with the state-of-the-art HER metal-based molecular and LD catalysts.

LD nanohybrids	Onset potential (mV vs RHE)	Ref
Mo_2CT_x/2H-MoS_2	-150	14
GD-WS_2 2D-NH	-210	15
graphene/WS_2/WO_3	-96	16
PAH@Rh-NSNSs/CNT	-1	17
$Sc_3N@D_3(6140)$-C_{68}	-38	**This work**

Table S2. Comparison of the mass activity of $Sc_3N@D_3(6140)$-C_{68} with the state-of-the-art HER metal-based LD catalysts.

LD nanohybrids	Mass activity ($A \cdot mg^{-1}$)	Ref
CoP NSs	1.51	18
G-Pt4Ni/GF	2.25	19
Ru/MWCNTs	3.75	20
Pt/f-MWCNTs	18.75	21
$Sc_3N@D_3(6140)$-C_{68}	1.75	**This work**

Table S3. Energies and Free Energies (in eV) Computed for H_2 Release from Hydrogenated Fullerenes.

Compound	$\Delta E(H_2)$[a)]	$\Delta G(H_2)$[a)]	$-\Delta G_{H^*}$[b)] (m=2)	$-\Delta G_{H^*}$[b)] (m=12)
$C_{60}H_2$	0.17	-0.37	-0.16	+0.06
$Sc_3N@C_{68}H_2$	0.37	-0.20	-0.06	+0.13
$Sc_3N@C_{80}H_2$	-0.05	-0.68	-0.27	-0.17

a) Values for the $Sc_3N@C_{2n}H_2$ -> $Sc_3N@C_{2n}$ + H_2 process; b) Determined as ΔG_{H^*} = (1/m) $E(M@C_{2n}H_m)$ – $E(M@C_{2n})$ – m/2 $E(H_2)$ +0.24. The lowest in energy adsorption sites are represented in Figure 4. The optimal location of H atoms for m=12 was obtained directly as neutral form see Figure S9.

References

1. Ceron, M. R.; Li, F. F.; Echegoyen, L., *Chem. Eur. J.* **2013,** 19 (23), 7410-7415.
2. Ceron, M. R.; Izquierdo, M.; Alegret, N.; Valdez, J. A.; Rodriguez-Fortea, A.; Olmstead, M. M.; Balch, A. L.; Poblet, J. M.; Echegoyen, L., *Chem. Commun.* **2016,** 52 (1), 64-67.
3. Stevenson, S.; Stephen, R. R.; Amos, T. M.; Cadorette, V. R.; Reid, J. E.; Phillips, J. P., Synthesis and purification of a metallic nitride fullerene BisAdduct: Exploring the reactivity of $Gd_3N@C_{80}$. *J. Am. Chem. Soc.* **2005**, 127 (37), 12776-12777.
4. Shen, W. Q.; Bao, L. P.; Hu, S. F.; Gao, X. J.; Xie, Y. P.; Gao, X. F.; Huang, W. H.; Lu, X., Isolation and Crystallographic Characterization of $Lu_3N@C_{2n}$ (2n=80-88): Cage Selection by Cluster Size. *Chem. Eur. J.* **2018,** *24* (62), 16692-16698.
5. Popov, A. A.; Dunsch, L., Structure, stability, and cluster-cage interactions in nitride clusterfullerenes $M_3N@C_{2n}$ (M = Sc, Y; 2n=68-98): a density functional theory study. *J. Am. Chem. Soc.* **2007,** *129* (38), 11835-11849.
6. Kibsgaard, J.; Tsai, C.; Chan, K.; Benck, J. D.; Norskov, J. K.; Abild-Pedersen, F.; Jaramillo, T. F., *Energy Environ. Sci.* **2015,** 8 (10), 3022-3029.
7. Masa, J.; Weide, P.; Peeters, D.; Sinev, I.; Xia, W.; Sun, Z. Y.; Somsen, C.; Muhler, M.; Schuhmann, W., *Adv. Energy Mater.* **2016,** 6 (6), 1502313.
8. Te Velde, G.; Bickelhaupt, F. M.; Baerends, E. J.; Guerra, C. F.; Van Gisbergen, S. J. A.; Snijders, J. G.; Ziegler, T., *J. Comp. Chem.* **2001,** 22 (9), 931-967.
9. Grimme, S.; Ehrlich, S.; Goerigk, L., *J. Comp. Chem.* **2011,** 32 (7), 1456-1465.
10. Andzelm, J.; Kolmel, C.; Klamt, A., *J. Chem. Phys.* **1995,** 103 (21), 9312-9320.
11. Klamt, A.; Schuurmann, G., *J . Chem. Soc . Perkin Trans .* **1993,** (5), 799-805.
12. Poblet, J. M.; Lopez, X.; Bo, C., *Chem. Soc. Rev.* **2003,** 32 (5), 297-308.
13. Soriano-Lopez, J.; Musaev, D. G.; Hill, C. L.; Galan-Mascaros, J. R.; Carbo, J. J.; Poblet, J. M., *J. Catal.* **2017,** 350, 56-63.
14. Lim Garrick, K.Handoko, A.; Johnson, L.; Meng, X.; Subramanian, G.; Anasori, B.; Gogotsi, Y.; Vojyodic, A.; Seh, Wei., *ACS Nano* **2020**, 14, 11, 16140–16155
15. Yao, Y.; Jin, Z. W.; Chen, Y. H.; Gao, Z. F.; Yan, J. Q.; Liu, H. B.; Wang, J. Z.; Li, Y. L.; Liu, S. Z., *Carbon* **2018,** 129, 228-235.
16. Chen, Y. T.; Ren, R.; Wen, Z. H.; Ci, S. Q.; Chang, J. B.; Mao, S.; Chen, J. H., *Nano Energy* **2018,** 47, 66-73.
17. Bai, J.; Xing, S. H.; Zhu, Y. Y.; Jiang, J. X.; Zeng, J. H.; Chen, Y., *J. Power Sources* **2018,** 385, 32-38.
18. Zhang, C.; Huang, Y.; Yu, Y. F.; Zhang, J. F.; Zhuo, S. F.; Zhang, B., *Chem. Sci.* **2017,** 8 (4), 2769-2775.
19. Yu, X. W.; Zhang, M.; Tong, Y.; Li, C.; Shi, G. Q., *Adv. Energy Mater.* **2018,** 8 (21), 1800403.
20. Zhang, W. Q.; Zhang, X.; Chen, L.; Dai, J. Y.; Ding, Y.; Ji, L. F.; Zhao, J.; Yan, M.; Yang, F. C.; Chang, C. R.; Guo, S. J., *ACS Catal.* **2018,** 8 (9), 8092-8099.
21. Ji, J. P.; Zhang, Y. P.; Tang, L. B.; Liu, C. Y.; Gao, X. H.; Sun, M. H.; Zheng, J. C.; Ling, M.; Liang, C. D.; Lin, Z., *Nano Energy* **2019,** 63, 103849.